

Communication

Influence of Surface Treatments on Urea Detection Using Si Electrolyte-Gated Transistors with Different Gate Electrodes

Wonyeong Choi ¹, Seonghwan Shin ¹, Jeonghyeon Do ¹, Jongmin Son ¹, Kihyun Kim ²
and Jeong-Soo Lee ^{1,3,*}

¹ Department of Electrical Engineering, Pohang University of Science and Technology (POSTECH), Pohang 37673, Republic of Korea; pathfinder@postech.ac.kr (W.C.); ssh3290a@postech.ac.kr (S.S.); toaru124@postech.ac.kr (J.D.); jmson@postech.ac.kr (J.S.)

² Division of Electronics Engineering, Jeonbuk National University, Jeonju 54896, Republic of Korea; kihyun.kim@jbnu.ac.kr

³ Innovative General Electronic Sensor Technology (i-GEST) Co., Ltd., Pohang 37673, Republic of Korea

* Correspondence: ljs6951@postech.ac.kr

Abstract: We investigated the impact of surface treatments on Si-based electrolyte-gated transistors (EGTs) for detecting urea. Three types of EGTs were fabricated with distinct gate electrodes (Ag, Au, Pt) using a top-down method. These EGTs exhibited exceptional intrinsic electrical properties, including a low subthreshold swing of 80 mV/dec, a high on/off current ratio of 10^6 , and negligible hysteresis. Three surface treatment methods ((3-amino-propyl) triethoxysilane (APTES) and glutaraldehyde (GA), 11-mercaptopundecanoic acid (11-MUA), 3-mercaptopropionic acid (3-MPA)) were individually applied to the EGTs with different gate electrodes (Ag, Au, Pt). Gold nanoparticle binding tests were performed to validate the surface functionalization. We compared their detection performance of urea and found that APTES and GA exhibited the most superior detection characteristics, followed by 11-MUA and 3-MPA, regardless of the gate metal. APTES and GA, with the highest pKa among the three surface treatment methods, did not compromise the activity of urease, making it the most suitable surface treatment method for urea sensing.

Keywords: biologically active field-effect transistor; electrolyte-gated transistor; enzyme sensor; pKa; urea detection



Citation: Choi, W.; Shin, S.; Do, J.; Son, J.; Kim, K.; Lee, J.-S. Influence of Surface Treatments on Urea Detection Using Si Electrolyte-Gated Transistors with Different Gate Electrodes. *Micromachines* **2024**, *15*, 621. <https://doi.org/10.3390/mi15050621>

Academic Editors: Fuze Jiang and Ha-Duong Ngo

Received: 15 April 2024

Revised: 2 May 2024

Accepted: 2 May 2024

Published: 5 May 2024



Copyright: © 2024 by the authors. Licensee MDPI, Basel, Switzerland. This article is an open access article distributed under the terms and conditions of the Creative Commons Attribution (CC BY) license (<https://creativecommons.org/licenses/by/4.0/>).

1. Introduction

Field-effect transistor (FET) biosensors have emerged as one of the most popular electric biosensors, renowned for their exceptional sensitivity, rapid response times, capacity for miniaturization, and cost efficiency [1,2]. These benefits stem from their operational principle, which relies on the gating effect of biochemical recognition on the sensing surface. Among FET sensors, electrolyte-gated transistors (EGTs) hold a leading position due to their high sensitivity [3–7]. EGTs utilize the gate electrode as the sensing surface, offering a broad sensing area and a high density of receptors, thereby achieving enhanced sensitivity.

EGTs have the potential to detect a wide range of analytes, depending on the receptors immobilized on the gate electrode. These analytes include pH, which is crucial in biomedical and environmental monitoring due to its impact on cellular function and ecological health [8]. Antigens are another key target, particularly in immunodiagnostic applications for detecting diseases such as COVID-19 [9]. DNA detection is essential in genetic analysis and diagnostics, aiding in disease identification and personalized medicine [10–12]. Enzyme sensors, in particular, have garnered significant attention for their various implications, such as medical diagnostics, food safety, and environmental monitoring [13–15].

In the field of enzyme sensors, enzymes serve as the bio-recognition elements, enabling the selective detection of target analytes. The immobilization of enzymes onto the sensing surface is a crucial step, as the immobilization process influences critical aspects such as the

accommodation of bio-recognition elements, preservation of their activity, and resistance against nonspecific interactions [16,17]. Therefore, in EGTs where the gate electrode is used as the sensing surface, the selection of suitable surface treatments and gate electrodes plays a pivotal role. Surprisingly, there have been few studies on the optimal combinations of surface treatments and gate electrodes, leaving an ideal material or immobilization method for biological sensing largely undefined.

To address this gap, we conducted a comparative study on surface treatment methods and gate electrodes for detecting urea. Urea is a key indicator of renal function in medical diagnostics, with abnormal levels indicating potential health issues [18]. We applied three surface treatment methods ((3-amino-propyl) triethoxysilane (APTES) and glutaraldehyde (GA), 11-mercaptopundecanoic acid (11-MUA), 3-mercaptopropionic acid (3-MPA)) to EGTs with gate electrodes made of three different types of metals (Ag, Au, Pt), and validated the surface functionalization using gold nanoparticles (AuNPs). Subsequently, we compared the detection performance to identify the most effective immobilization method and gate electrode.

2. Materials and Methods

2.1. Material Preparation

Urease from Jack Beans (Type III, powder, 20,000 units/g), urea (molecular biology grade, powder), phosphate-buffered saline (PBS, pH 7.4), (3-amino-propyl) triethoxysilane (APTES, 99%), anhydrous ethanol (200 proof, 99.5%), glutaraldehyde (GA, 50%), 11-mercaptopundecanoic acid (11-MUA, 98%), 3-mercaptopropionic acid (3-MPA, 99%), 1-ethyl-3-(3-dimethylaminopropyl)carbodiimide (EDAC, 98%), N-hydroxysuccinimide (NHS, 98%), IgG from mouse serum (95%), anti-mouse IgG conjugated with AuNP, glucose, ascorbic acid (AA), and KCl were purchased from Sigma-Aldrich (Burlington, VT, USA). Urea and other biomolecules, such as glucose, AA, and KCl, were dissolved in the $1 \times$ PBS solution. We denoted the concentration of urea with $pUrea$ ($pUrea = -\log_{10}[Urea]$).

2.2. Fabrication of EGTs

Using a top-down approach, the EGTs were fabricated on a silicon-on-insulator wafer (p-type, $10 \Omega \cdot \text{cm}$ (100)) (Figure 1). Initially, a 140 nm-thick top silicon layer was thinned to 100 nm through thermal oxidation. The active regions (source, drain, channel) were defined using a KrF scanner and an inductively coupled plasma reactive-ion etching (ICP-RIE) process. To minimize etching-induced damage and serve as a blocking layer for the ion implantation process, a 20 nm sacrificial oxide was grown using a thermal furnace. Arsenic ions at a dose of $5 \times 10^{15}/\text{cm}^2$ and an energy of 60 keV were implanted into the source and drain regions, followed by rapid thermal annealing (RTA) at 1000°C for 20 s. Subsequently, a 5 nm gate oxide layer was grown using thermal oxidation. The gate electrode and source/drain transmission lines were formed using a lift-off process with 500 nm of Ag, Au, or Pt. Finally, a 2 μm -thick SU-8 passivation layer was applied for electrical isolation, except for the gate sensing area, channel, and contact pads. The passivation layer prevents the current flow from the source and drain regions to the aqueous solution and gate region during measurement.

2.3. Electrical Characterization

Utilizing a semiconductor parameter analyzer (Keithley 4200, Keithley, Solon, OH, USA), the electrical characteristics were measured. The gate voltage (V_G) was applied through a buffer solution, and the drain current (I_D) was measured at a constant drain voltage (V_D) of 0.1 V, with source and body voltages (V_S and V_B) set to 0 V. The I_D - V_G characterizations were conducted after a 10 min exposure of the 20 μL target solution. I_D was restricted to 10^{-7} A to prevent device degradation during the characterization.

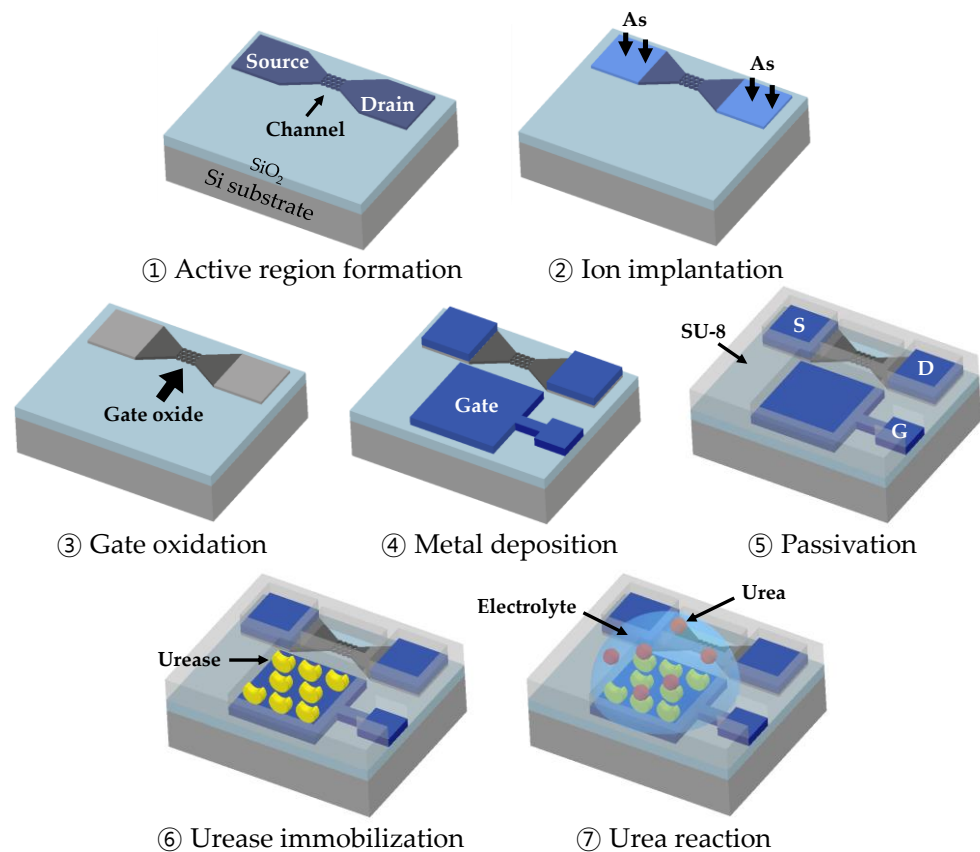


Figure 1. Fabrication and characterization steps of the Si-based electrolyte-gated transistor (EGT).

2.4. Functionalization of EGTs

Three distinct materials were employed for the immobilization of urease on EGTs, as listed in Table 1. For the surface treatment using APTES and GA, a UV/ozone treatment with an intensity of $200 \mu\text{W}/\text{cm}^2$ for 90 s was initially conducted on the device. After exposure to APTES at 55°C for 1 min, the device was rinsed with anhydrous ethanol and immersed in a 2.5% GA solution ($1 \times \text{PBS}$, pH 7.4) for 90 min. Then, it was washed with $1 \times \text{PBS}$ and DI water (DIW) and dried using N_2 blowing. The ethoxy group (OCH_2CH_3-) of APTES bound onto the gate electrode, and the remaining amine group (NH_2-) coupled with the aldehyde group ($\text{CHO}-$) of GA, which can bind to urease. Conjugate length of APTES and GA was 1.5 nm [19,20]. The pKa values of APTES and GA are both 10 [21,22], which indicates minimal impact on the pH of the buffer.

Table 1. Materials employed for urease immobilization and their characteristics.

Material	Functional Group		Length	pKa
	Binding with Gate	Binding with Receptor		
APTES and GA [19–22]	Ethoxy group (OCH_2CH_3-)	Amine group (NH_2-)	1.5 nm	10
11-MUA [23–27]	Thiol group ($\text{SH}-$)	Carboxyl group ($\text{COOH}-$)	1.6 nm	6.5
3-MPA [28,29]	Thiol group ($\text{SH}-$)	Carboxyl group ($\text{COOH}-$)	0.6 nm	5.2

11-MUA is a widely-used substance for metal binding [23–25]. The thiol group ($\text{SH}-$) of 11-MUA binds to the gate metal, and the remaining carboxyl group ($\text{COOH}-$) attaches to urease. The length of 11-MUA is 1.6 nm [26], and its pKa is 6.5 [27], which is lower

than that of APTES and GA. This lower pKa is attributed to the low affinity of COOH⁻ for hydrogen ions (H⁺), facilitating easy dissociation.

The final material employed was 3-MPA, which binds to metals through the thiol group (SH⁻) and attaches to urease via the carboxyl group (COOH⁻) in the same manner as 11-MUA. The length of 3-MPA is 0.6 nm [28], the shortest among the three surface modifications, and its pKa of 5.2 [29] is even lower than that of 11-MUA.

The surface treatments for 11-MUA and 3-MPA were similar, as follows. Initially, the devices were immersed in a 20 mM solution of 11-MUA or 3-MPA in an ethanol base for 18 h. Then, the devices were rinsed with ethanol and DIW and dried with N₂ blowing. Subsequently, the devices were incubated in a solution containing 20 mM EDAC or 20 mM NHS in a 1 × PBS base for 1 h to activate 11-MUA or 3-MPA, respectively. Finally, the devices were rinsed with 1 × PBS and DIW and dried with N₂ blowing. After the surface treatments described above, a urease solution (10 mg/mL, 1 × PBS, pH 7.4) was applied to those devices for 18 h at 4 °C in a humid environment, followed by rinsing with 1 × PBS and DIW and drying with N₂ blowing.

AuNP binding tests were performed to evaluate the surface functionalization for different gate materials. A solution of mouse IgG (1 mg/mL, 1 × PBS) was applied to the devices in a humid environment at 4 °C for 18 h, rinsed with 1 × PBS and DIW, and dried with N₂ blowing. Then, a solution of anti-mouse IgG conjugated with AuNP of 10 nm diameter was applied to the metal for 30 min, rinsed, and dried. The binding of AuNPs was examined using scanning electron microscopy (SEM). As shown in Figure 2, the average densities of AuNPs were in the ranges of 450–550 μm² for different surface treatments and gate metals. Each data point corresponds to the average measurement obtained from five samples.

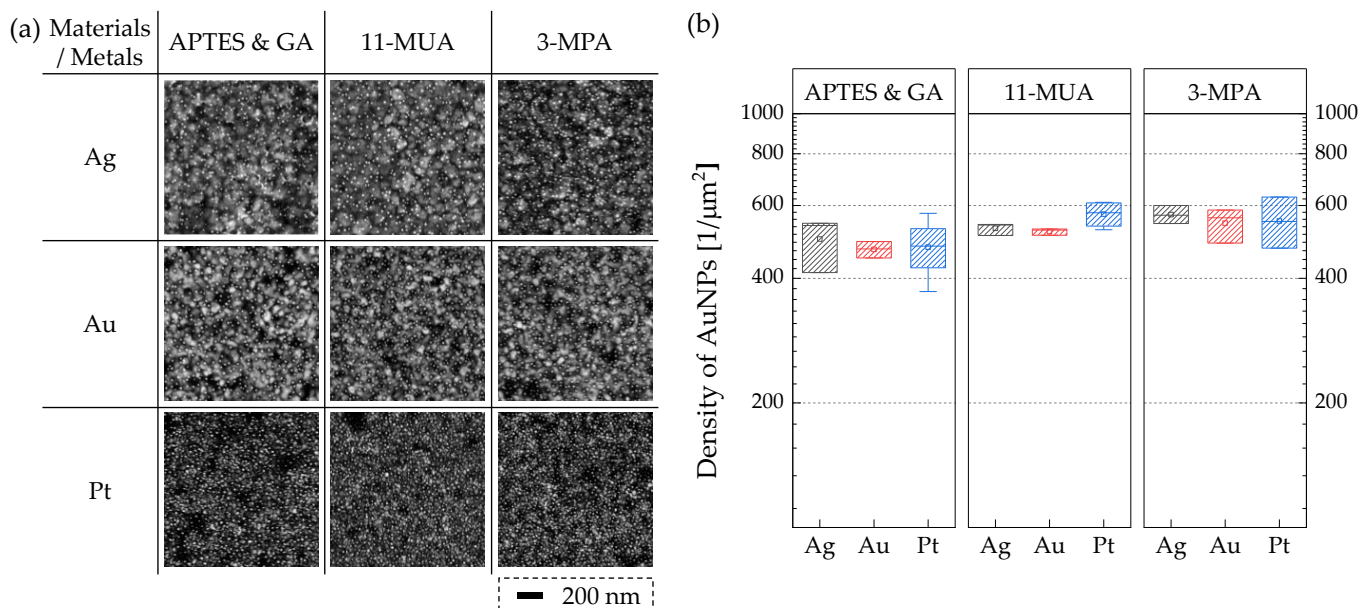


Figure 2. (a) Scanning electron microscopy (SEM) images and (b) the density of AuNPs immobilized on Ag, Au, and Pt metals for different surface treatments.

3. Results and Discussion

3.1. Intrinsic Electrical Characteristics

Figure 3 shows the intrinsic transfer curve (I_D vs. V_G) for EGTs with different gate metals. Regardless of the gate metal, these devices exhibit outstanding characteristics, including a low subthreshold swing (SS) of 80 mV/dec, high on/off current ratio of 10^6 , and negligible hysteresis of less than 10 mV. The threshold voltage (V_{TH}) is characterized as low as 0.55 V for Ag, 0.65 V for Au, and 0.7 V for Pt, respectively, which is mainly attributed to the metal work-function difference [30].

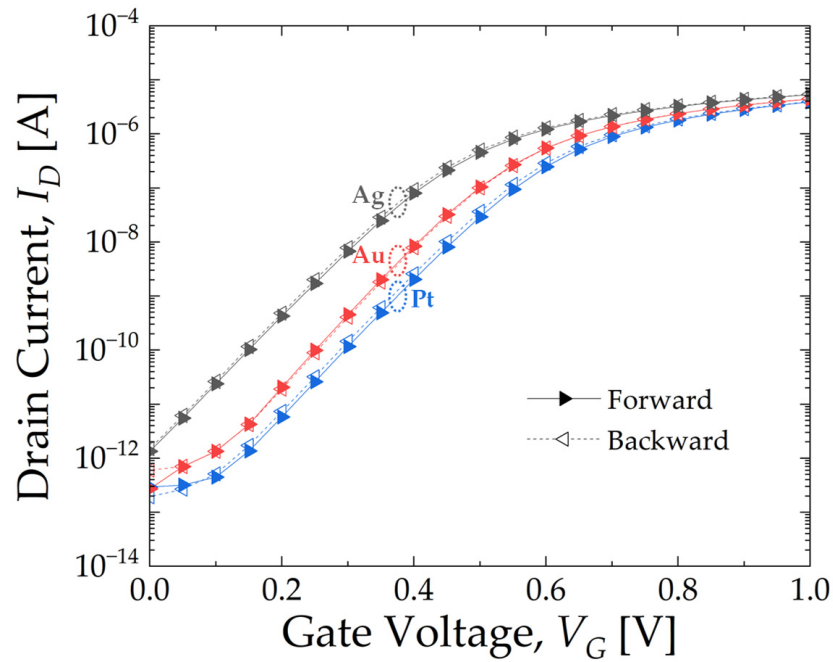


Figure 3. I_D - V_G characteristics of fabricated electrolyte-gated transistors (EGTs) with Ag, Au, and Pt gate electrodes for forward and backward sweeps at $V_D = 0.1$ V in $1 \times$ PBS solution.

3.2. Urea Sensing Characteristics

Figure 4 shows the real-time responses for urea with urease-functionalized EGTs for 600 s. Compared with the negative samples ($1 \times$ PBS without urea, half-empty symbols), those exposed to a urea solution (pUrea 0.5, filled symbols) decrease monotonously and then saturate.

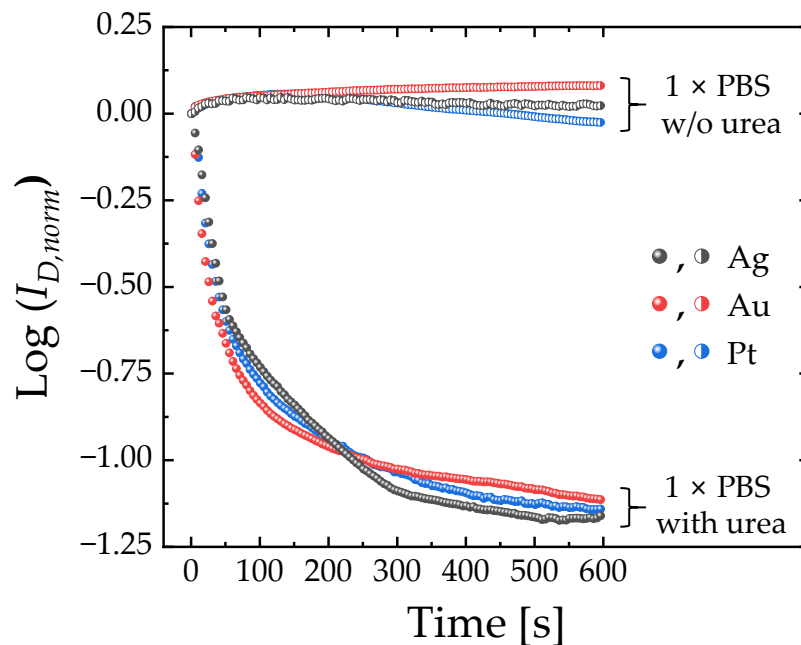


Figure 4. Real-time responses for detecting urea (pUrea 0.5) in urease-functionalized electrolyte-gated transistors (EGTs) using 3-amino-propyl triethoxysilane (APTES) and glutaraldehyde (GA). The normalized drain current ($I_{D, norm}$) was characterized at a fixed V_G of 0.3 V and V_D of 0.1 V. $I_{D, norm}$ represents the ratio of I_D to I_{D0} , where I_{D0} denotes the initial I_D measured at $t = 0$ s.

The voltage-related response (R_V) and the current-related response (R_I) are defined as follows [15,31,32]:

$$R_V = V_{G1} - V_{G0}, \tag{1}$$

$$R_I = \frac{I_{D0} - I_{D1}}{I_{D1}}, \tag{2}$$

where V_{G0} and V_{G1} represent gate voltages at a fixed I_{D0} of 3 nA before and after the reaction, respectively. I_{D0} and I_{D1} represent drain currents at a fixed V_{G0} of 0.3 V before and after the reaction, respectively.

Figure 5 illustrates the correlation between R_V and pUrea based on three surface treatment methods (APTES and GA, 11-MUA, 3-MPA) for EGTs with three gate metals ((a) Ag, (b) Au, (c) Pt). Each point represents the average of five different devices. In all conditions, it can be observed that as the urea concentration increases, the signal amplifies until reaching saturation. Regardless of the gate metal, a similar trend of higher R_V values in the order of APTES and GA, 11-MUA, and 3-MPA was observed.

Figure 6 presents the extracted metrics from the R_V vs. pUrea results of Figure 5. Figure 6a represents the $R_{V,max}$, which is defined as the maximum value from the fitted curve. Figure 6b shows the urea sensitivity related to R_V (S_V), determined by the slope of the logistic-fitted line of R_V [15]. Figure 6c depicts the limit of detection (LOD) of R_V , defined using the 3σ method from the logistic trend line [33]. It can be observed across all metrics ($R_{V,max}$, S_V , LOD) that APTES and GA exhibits the most superior characteristics, followed by 11-MUA and 3-MPA, regardless of the metal type.

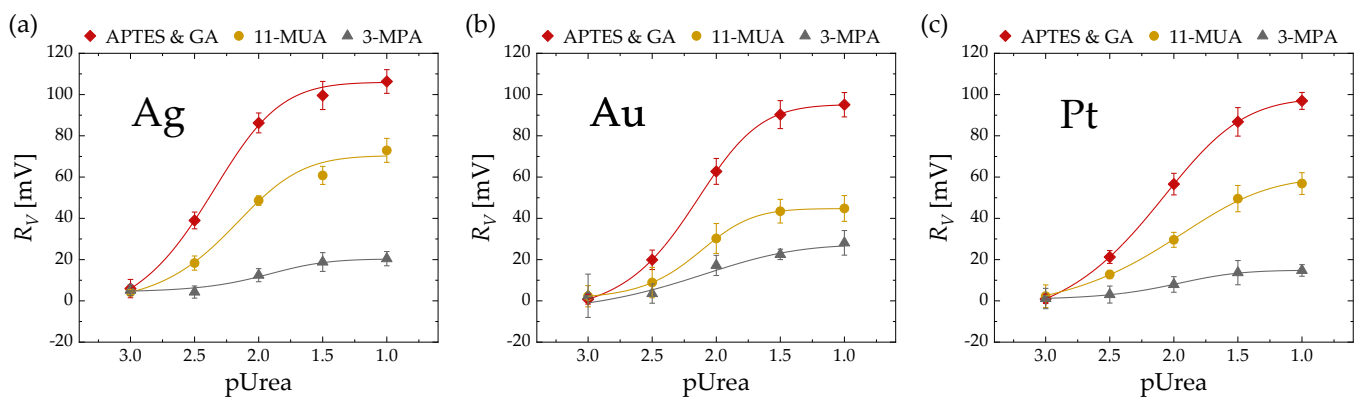


Figure 5. R_V vs. pUrea based on three surface treatment methods (APTES & GA, 11-MUA, 3-MPA) with EGTs featuring (a) Ag, (b) Au, and (c) Pt gate metals. The solid curves represent logistic fitted lines.

Figure 7 illustrates the correlation between R_I and pUrea based on three surface treatment methods (APTES and GA, 11-MUA, 3-MPA) for EGTs with three gate metals ((a) Ag, (b) Au, (c) Pt). Each point represents the average of five different devices. Regardless of the gate metal, a similar trend of higher R_I values in the order of APTES and GA, 11-MUA, and 3-MPA was observed.

Figure 8 presents the extracted metrics from the R_I vs. pUrea results of Figure 7. Figure 8a, Figure 8b, and Figure 8c depict $R_{I,max}$, urea sensitivity related to R_I (S_I) and LOD, respectively, based on the gate metal and surface treatment method. Consistent with the extraction based on R_V , it can be observed across all metrics ($R_{I,max}$, S_I , LOD) that regardless of the metal type, APTES and GA exhibits the most superior characteristics, followed by 11-MUA and 3-MPA.

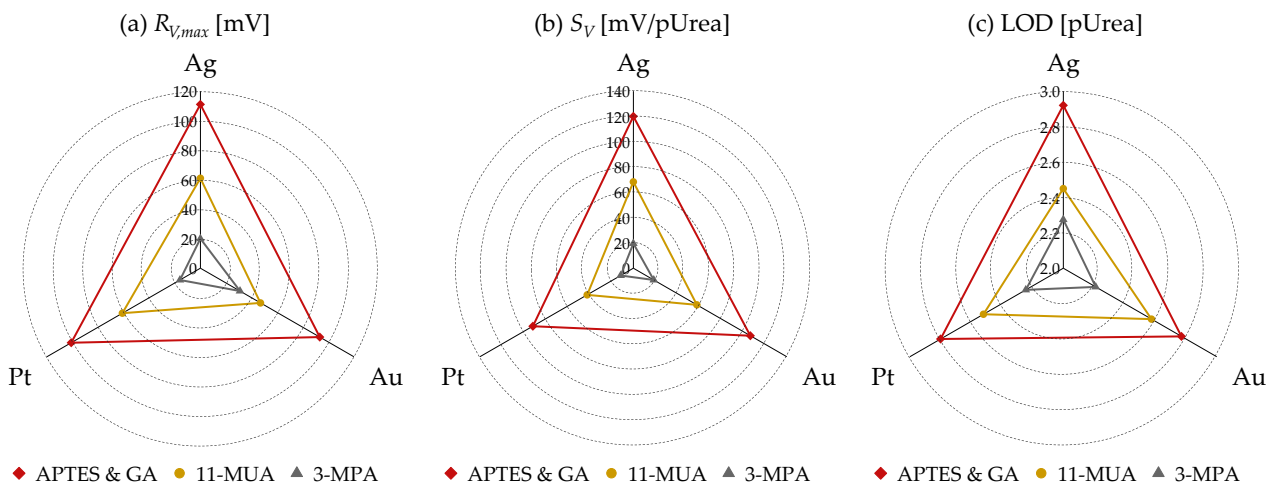


Figure 6. (a) $R_{V,max}$, (b) S_V , and (c) limit of detection (LOD) based on three surface treatment methods (APTES and GA, 11-MUA, 3-MPA) and three gate metals (Ag, Au, Pt) extracted from R_V vs. pUrea relationship in Figure 5.

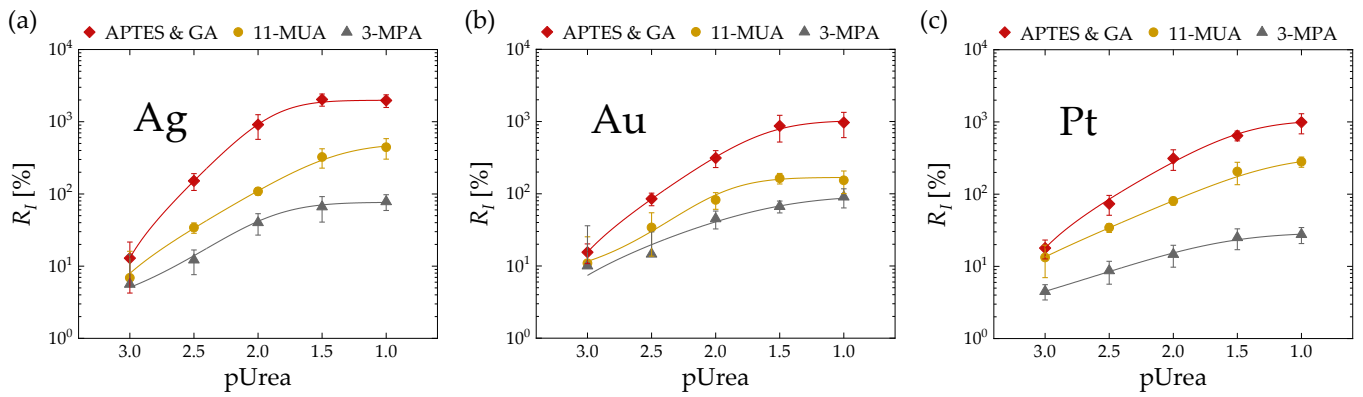


Figure 7. R_I vs. pUrea based on three surface treatment methods (APTES and GA, 11-MUA, 3-MPA) with electrolyte-gated transistors (EGTs) featuring (a) Ag, (b) Au, and (c) Pt gate metals. The solid curves represent logistic-fitted lines.

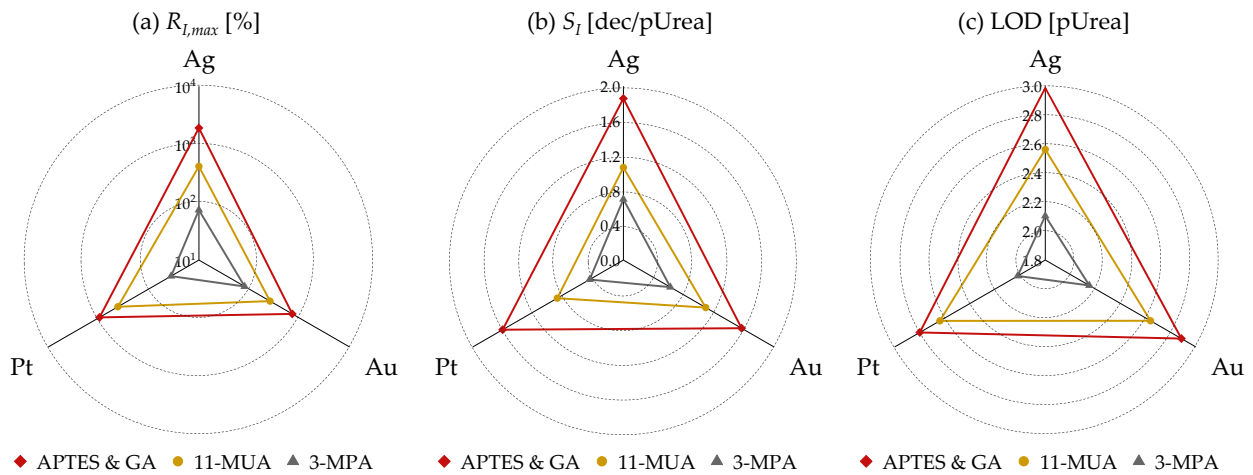


Figure 8. (a) $R_{I,max}$, (b) S_I , and (c) limit of detection (LOD) based on three surface treatment methods (APTES and GA, 11-MUA, 3-MPA) and three gate metals (Ag, Au, Pt) extracted from R_I vs. pUrea relationship in Figure 7.

Tendency observed among surface treatment materials stems from the relationship between their respective pKa values and urease activity. The activity of all enzymes, including urease, varies with pH. The jack bean urease used in this study exhibits maximum activity at pH 7.5, decreasing as the pH decreases [34]. Both 11-MUA (pKa 6.5) and 3-MPA (pKa 5.2) possess carboxy terminals (COOH⁻), making them prone to the easy decomposition of H⁺ ions, thus acidifying the surrounding solution (Figure 9). This acidity diminishes the activity of urease, consequently reducing the signal magnitude [35]. In contrast, APTES and GA (pKa 10) feature amine terminals (NH₂) that resist the release of H⁺ ions, thus having minimal influence on the solution's pH. Consequently, using APTES and GA does not compromise urease activity, making it the most suitable surface treatment method for urea sensing.

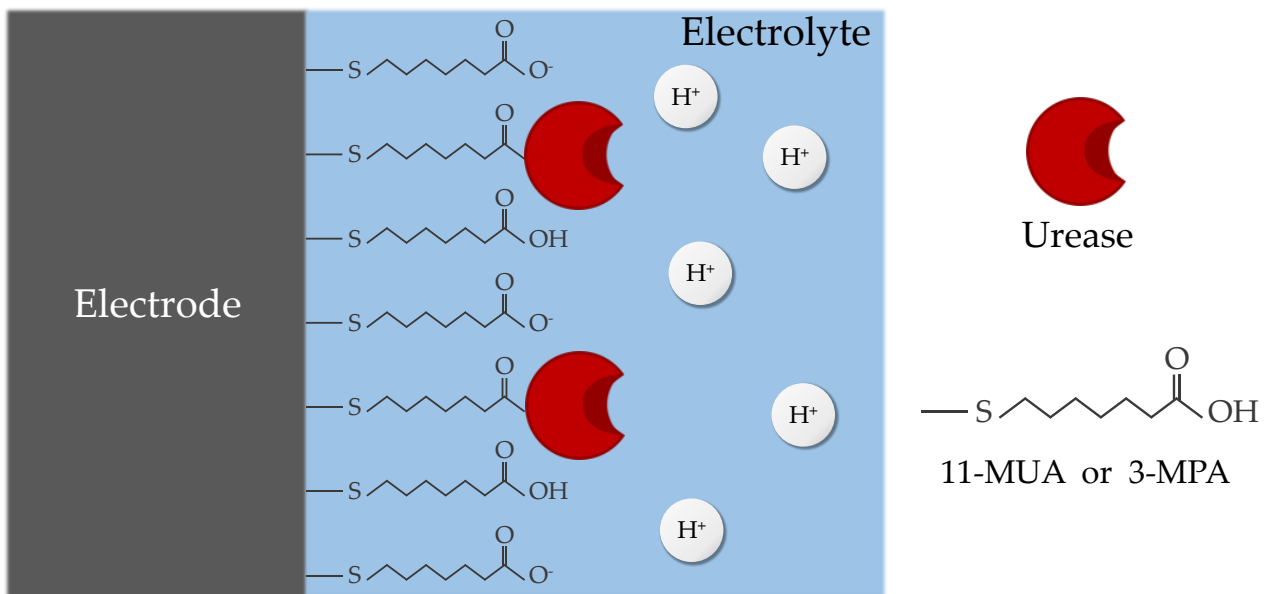


Figure 9. Schematic image of urease immobilized on the gate electrode using 11-MUA or 3-MPA. The carboxyl terminals decompose H⁺ ions, thereby lowering the pH of the surrounding electrolyte.

3.3. Selectivity Test

To demonstrate the specific detection of urea, a selectivity test was conducted (Figure 10). Each data point corresponds to the average measurement obtained from five devices. The immobilization of urease was carried out using APTES and GA, which was identified as the most effective surface treatment method. For reacting substances commonly found in blood vessels, such as glucose, ascorbic acid, and KCl, only R_V values smaller than 10 mV were observed regardless of gate metals (Ag, Au, Pt). Additionally, when a high concentration (316 mM) of urea was reacted with the EGTs without urease immobilization, the resulting R_V was less than one-third of the value observed when reacting with a 100 times lower concentration (3.16 mM) of urea on the EGTs with urease immobilization. This confirmed the successful immobilization of urease on the EGTs and reiterated the specific detection of urea through the reaction between urease and urea using all gate metals (Ag, Au, Pt).

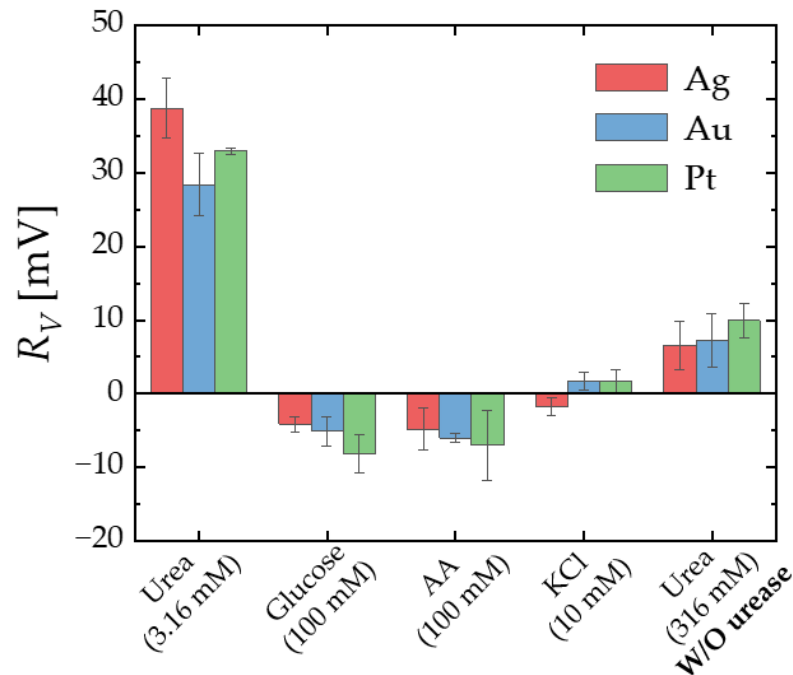


Figure 10. Control experiments: R_V for urea (3.16 mM, pUrea 2.5), glucose (100 mM), AA (100 μ M), and KCl (10 mM) with urease functionalized electrolyte-gated transistors (EGTs), and R_V for urea (316 mM, pUrea 0.5) with unmodified EGTs.

4. Conclusions

We conducted a study on the impact of surface treatment for detecting urea on EGTs with different gate electrodes. Using AuNPs, we confirmed the effective immobilization of urease on Ag, Au, and Pt gate metals using APTES and GA, 11-MUA, and 3-MPA. Upon testing the signal responses for urea on the three metals with the three surface treatment methods, we found that APTES and GA consistently exhibited superior detection performance, irrespective of the metal used. This was attributed to the acidic nature of 11-MUA and 3-MPA, which reduced urease activity. Furthermore, it is known that not only urease but all enzymes have their optimal pH range; we anticipate that the same principles can be applied to other enzyme-based sensors.

Author Contributions: Conceptualization, W.C.; methodology, W.C. and K.K.; validation, W.C. and J.-S.L.; investigation, S.S. and J.D.; data curation, S.S. and J.S.; writing—original draft preparation, W.C., K.K. and J.-S.L.; writing—review and editing, W.C. and J.-S.L.; supervision J.-S.L. All authors have read and agreed to the published version of the manuscript.

Funding: This research was supported by the National R&D Program through the National Research Foundation of Korea (NRF) funded by the Ministry of Science and ICT (2020M3H2A107804521) and the Starting Growth Technological R&D Program (TIPS Program, (No. RS-2023-00258751)) funded by the Ministry of SMEs and Startups (MSS, Korea) in 2023.

Data Availability Statement: The data presented in this study are not available due to privacy.

Conflicts of Interest: Author Jeong-Soo Lee was employed by the company Innovative General Electronic Sensor Technology (i-GEST) Co., Ltd. The remaining authors declare that the research was conducted in the absence of any commercial or financial relationships that could be construed as a potential conflict of interest.

References

1. Gao, A.; Lu, N.; Dai, P.; Li, T.; Pei, H.; Gao, X.; Gong, Y.; Wang, Y.; Fan, C. Silicon-Nanowire-Based CMOS-Compatible Field-Effect Transistor Nanosensors for Ultrasensitive Electrical Detection of Nucleic Acids. *Nano Lett.* **2011**, *11*, 3974–3978. [[CrossRef](#)] [[PubMed](#)]
2. Zheng, G.; Patolsky, F.; Cui, Y.; Wang, W.U.; Lieber, C.M. Multiplexed electrical detection of cancer markers with nanowire sensor arrays. *Nat. Biotechnol.* **2005**, *23*, 1294–1301. [[CrossRef](#)] [[PubMed](#)]
3. Mulla, M.Y.; Tuccori, E.; Magliulo, M.; Lattanzi, G.; Palazzo, G.; Persaud, K.; Torsi, L. Capacitance-modulated transistor detects odorant binding protein chiral interactions. *Nat. Commun.* **2015**, *6*, 6010. [[CrossRef](#)] [[PubMed](#)]
4. Macchia, E.; Manoli, K.; Holzer, B.; Di Franco, C.; Ghittorelli, M.; Torricelli, F.; Alberga, D.; Mangiatordi, G.F.; Palazzo, G.; Scamarcio, G.; et al. Single-molecule detection with a millimetre-sized transistor. *Nat. Commun.* **2018**, *9*, 3223. [[CrossRef](#)] [[PubMed](#)]
5. Guo, K.; Wustoni, S.; Koklu, A.; Díaz-Galicia, E.; Moser, M.; Hama, A.; Alqahtani, A.A.; Ahmad, A.N.; Alhamlan, F.S.; Shuaib, M.; et al. Rapid single-molecule detection of COVID-19 and MERS antigens via nanobody-functionalized organic electrochemical transistors. *Nat. Biomed. Eng.* **2021**, *5*, 666–677. [[CrossRef](#)]
6. Kim, D.; Jin, B.; Kim, S.-A.; Choi, W.; Shin, S.; Park, J.; Shim, W.-B.; Kim, K.; Lee, J.-S. An Ultrasensitive Silicon-Based Electrolyte-Gated Transistor for the Detection of Peanut Allergens. *Biosensors* **2022**, *12*, 24. [[CrossRef](#)]
7. Macchia, E.; Sarcina, L.; Picca, R.A.; Manoli, K.; Di Franco, C.; Scamarcio, G.; Torsi, L. Ultra-low HIV-1 p24 detection limits with a bioelectronic sensor. *Anal. Bioanal. Chem.* **2019**, *412*, 811–818. [[CrossRef](#)] [[PubMed](#)]
8. Torricelli, F.; Adrahtas, D.Z.; Bao, Z.; Berggren, M.; Biscarini, F.; Bonfiglio, A.; Bortolotti, C.A.; Frisbie, C.D.; Macchia, E.; Malliaras, G.G.; et al. Electrolyte-gated transistors for enhanced performance bioelectronics. *Nat. Rev. Methods Prim.* **2021**, *1*, 66. [[CrossRef](#)]
9. Shin, S.; Kim, S.; Choi, W.; Do, J.; Son, J.; Kim, K.; Jang, S.; Lee, J.-S. Sensing Characteristics of SARS-COV-2 Spike Protein Using Aptamer-Functionalized Si-Based Electrolyte-Gated Field-Effect Transistor (EGT). *Biosensors* **2024**, *14*, 124. [[CrossRef](#)]
10. Hwang, M.T.; Heiranian, M.; Kim, Y.; You, S.; Leem, J.; Taqieddin, A.; Faramarzi, V.; Jing, Y.; Park, I.; van der Zande, A.M.; et al. Ultrasensitive detection of nucleic acids using deformed graphene channel field effect biosensors. *Nat. Commun.* **2020**, *11*, 1543. [[CrossRef](#)]
11. Campos, R.; Borme, J.; Guerreiro, J.R.; Machado, G., Jr.; Cerqueira, M.F.; Petrovykh, D.Y.; Alpuim, P. Attomolar Label-Free Detection of DNA Hybridization with Electrolyte-Gated Graphene Field-Effect Transistors. *ACS Sens.* **2019**, *4*, 286–293. [[CrossRef](#)] [[PubMed](#)]
12. Hajian, R.; Balderston, S.; Tran, T.; Deboer, T.; Etienne, J.; Sandhu, M.; Wauford, N.A.; Chung, J.-Y.; Nokes, J.; Athaiya, M.; et al. Detection of unamplified target genes via CRISPR-Cas9 immobilized on a graphene field-effect transistor. *Nat. Biomed. Eng.* **2019**, *3*, 427–437. [[CrossRef](#)] [[PubMed](#)]
13. Ohayon, D.; Nikiforidis, G.; Savva, A.; Giugni, A.; Wustoni, S.; Palanisamy, T.; Chen, X.; Maria, I.P.; Di Fabrizio, E.; Costa, P.M.F.J.; et al. Biofuel powered glucose detection in bodily fluids with an n-type conjugated polymer. *Nat. Mater.* **2019**, *19*, 456–463. [[CrossRef](#)] [[PubMed](#)]
14. Rissin, D.M.; Walt, D.R. Digital Concentration Readout of Single Enzyme Molecules Using Femtoliter Arrays and Poisson Statistics. *Nano Lett.* **2006**, *6*, 520–523. [[CrossRef](#)] [[PubMed](#)]
15. Choi, W.; Jin, B.; Shin, S.; Do, J.; Son, J.; Kim, K.; Lee, J.-S. Highly Sensitive Detection of Urea Using Si Electrolyte-Gated Transistor with Low Power Consumption. *Biosensors* **2023**, *13*, 565. [[CrossRef](#)] [[PubMed](#)]
16. Maghraby, Y.R.; El-Shabasy, R.M.; Ibrahim, A.H.; Azzazy, H.M.E.-S. Enzyme Immobilization Technologies and Industrial Applications. *ACS Omega* **2023**, *8*, 5184–5196. [[CrossRef](#)]
17. Sassolas, A.; Blum, L.J.; Leca-Bouvier, B.D. Immobilization strategies to develop enzymatic biosensors. *Biotechnol. Adv.* **2012**, *30*, 489–511. [[CrossRef](#)] [[PubMed](#)]
18. Botewad, S.N.; Gaikwad, D.K.; Girhe, N.B.; Thorat, H.N.; Pawar, P.P. Urea Biosensors: A Comprehensive Review. *Biotechnol. Appl. Biochem.* **2023**, *70*, 485–501. [[CrossRef](#)]
19. Salem, M.; Mauguén, Y.; Prangé, T. Revisiting glutaraldehyde cross-linking: The case of the Arg-Lys intermolecular doublet. *Acta Crystallogr. Sect. F Struct. Biol. Cryst. Commun.* **2010**, *66*, 225–228. [[CrossRef](#)]
20. Zhu, M.; Lerum, M.Z.; Chen, W. How To Prepare Reproducible, Homogeneous, and Hydrolytically Stable Aminosilane-Derived Layers on Silica. *Langmuir* **2011**, *28*, 416–423. [[CrossRef](#)]
21. Chiang, Y.; Kresge, A.J.; Krogh, E.T. Diphenylacetaldehyde and Its Enol: Determination of the Keto Enol and Hydration Equilibrium-Constants and the Pk_as of the Aldehyde, Enol, and Hydrate. Comparison with Sterically Hindered Systems. *J. Am. Chem. Soc.* **1988**, *110*, 2600–2607. [[CrossRef](#)]
22. Nolte, A.J.; Chung, J.Y.; Walker, M.L.; Stafford, C.M. In situ Adhesion Measurements Utilizing Layer-by-Layer Functionalized Surfaces. *ACS Appl. Mater. Interfaces* **2009**, *1*, 373–380. [[CrossRef](#)] [[PubMed](#)]
23. Wang, T.; Yang, Z.; Lei, C.; Lei, J.; Zhou, Y. An integrated giant magnetoimpedance biosensor for detection of biomarker. *Biosens. Bioelectron.* **2014**, *58*, 338–344. [[CrossRef](#)] [[PubMed](#)]
24. Dai, Y.; Wang, C.; Chiu, L.-Y.; Abbasi, K.; Tolbert, B.S.; Sauvé, G.; Yen, Y.; Liu, C.-C. Application of bioconjugation chemistry on biosensor fabrication for detection of TAR-DNA binding protein 43. *Biosens. Bioelectron.* **2018**, *117*, 60–67. [[CrossRef](#)] [[PubMed](#)]
25. Wu, N.-T.; Jiang, B.-S.; Lo, Y.-H.; Huang, J.-J. Investigation of streptavidin-ligand biochemical interactions by IGZO thin film transistors integrated with microfluidic channels. *Sens. Actuators B Chem.* **2018**, *262*, 418–424. [[CrossRef](#)]

26. Cecchet, F.; Rudolf, P.; Rapino, S.; Margotti, M.; Paolucci, F.; Baggerman, J.; Brouwer, A.M.; Kay, E.R.; Wong, J.K.Y.; Leigh, D.A. Structural, Electrochemical, and Photophysical Properties of a Molecular Shuttle Attached to an Acid-Terminated Self-Assembled Monolayer. *J. Phys. Chem. B* **2004**, *108*, 15192–15199. [[CrossRef](#)]
27. Yao, D.-J.; Yang, Y.-R.; Tai, C.-C.; Hsiao, W.-H.; Ling, Y.-C. A biochemical sensing system using an 11-MUA/calix[6]arene bilayer to sense amine vapors. *J. Micromech. Microeng.* **2007**, *17*, 1435–1441. [[CrossRef](#)]
28. Jennings, G.K.; Munro, J.C.; Yong, T.-H.; Laibinis, P.E. Effect of Chain Length on the Protection of Copper by *n*-Alkanethiols. *Langmuir* **1998**, *14*, 6130–6139. [[CrossRef](#)]
29. Zheng, H.; Hirose, Y.; Kimura, T.; Suye, S.-I.; Hori, T.; Katayama, H.; Arai, J.-I.; Kawakami, R.; Ohshima, T. L-Proline sensor based on layer-by-layer immobilization of thermostable dye-linked l-proline dehydrogenase and polymerized mediator. *Sci. Technol. Adv. Mater.* **2006**, *7*, 243–248. [[CrossRef](#)]
30. Zangmeister, C.D.; Picraux, L.B.; van Zee, R.D.; Yao, Y.; Tour, J.M. Energy-level alignment and work function shifts for thiol-bound monolayers of conjugated molecules self-assembled on Ag, Cu, Au, and Pt. *Chem. Phys. Lett.* **2007**, *442*, 390–393. [[CrossRef](#)]
31. Shoorideh, K.; Chui, C.O. Optimization of the Sensitivity of FET-Based Biosensors via Biasing and Surface Charge Engineering. *IEEE Trans. Electron Devices* **2012**, *59*, 3104–3110. [[CrossRef](#)]
32. Hideshima, S.; Hinou, H.; Ebihara, D.; Sato, R.; Kuroiwa, S.; Nakanishi, T.; Nishimura, S.-I.; Osaka, T. Attomolar Detection of Influenza A Virus Hemagglutinin Human H1 and Avian H5 Using Glycan-Blotted Field Effect Transistor Biosensor. *Anal. Chem.* **2013**, *85*, 5641–5644. [[CrossRef](#)] [[PubMed](#)]
33. Gao, A.; Lu, N.; Wang, Y.; Li, T. Robust ultrasensitive tunneling-FET biosensor for point-of-care diagnostics. *Sci. Rep.* **2016**, *6*, 22554. [[CrossRef](#)] [[PubMed](#)]
34. Cesareo, S.D.; Langton, S.R. Kinetic properties of *Helicobacter pylori* urease compared with jack bean urease. *FEMS Microbiol. Lett.* **1992**, *99*, 15–22. [[CrossRef](#)]
35. Silva, G.O.; Mulato, M. Urea Detection Using Commercial Field Effect Transistors. *ECS J. Solid State Sci. Technol.* **2018**, *7*, Q3014–Q3019. [[CrossRef](#)]

Disclaimer/Publisher’s Note: The statements, opinions and data contained in all publications are solely those of the individual author(s) and contributor(s) and not of MDPI and/or the editor(s). MDPI and/or the editor(s) disclaim responsibility for any injury to people or property resulting from any ideas, methods, instructions or products referred to in the content.